



Lawrence Berkeley Laboratory

UNIVERSITY OF CALIFORNIA

EARTH SCIENCES DIVISION

RECEIVED
LAWRENCE
BERKELEY LABORATORY

FEB 18 1983

To be published in the Journal of Geophysical Research
LIBRARY AND DOCUMENTS SECTION

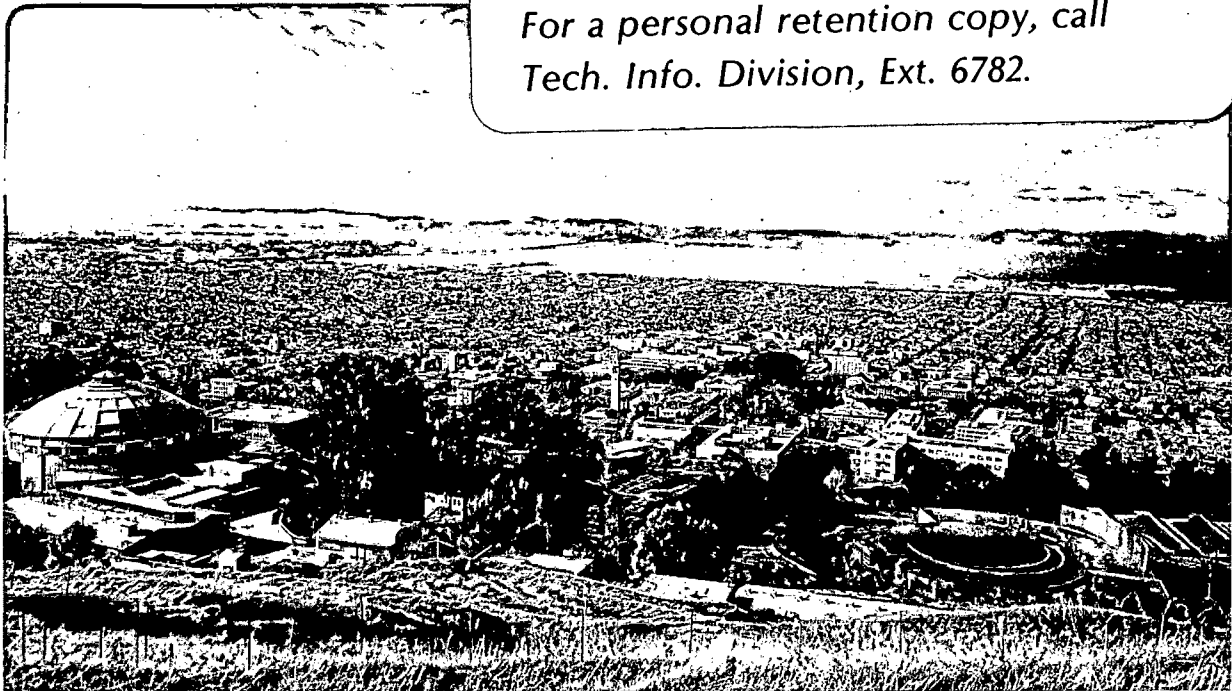
THE DEPENDENCE OF FRACTURE MECHANICAL AND
FLUID FLOW PROPERTIES ON FRACTURE ROUGHNESS
AND SAMPLE SIZE

Y.W. Tsang and P.A. Witherspoon

May 1982

TWO-WEEK LOAN COPY

*This is a Library Circulating Copy
which may be borrowed for two weeks.
For a personal retention copy, call
Tech. Info. Division, Ext. 6782.*



LBL-14087
c. 2

DISCLAIMER

This document was prepared as an account of work sponsored by the United States Government. While this document is believed to contain correct information, neither the United States Government nor any agency thereof, nor the Regents of the University of California, nor any of their employees, makes any warranty, express or implied, or assumes any legal responsibility for the accuracy, completeness, or usefulness of any information, apparatus, product, or process disclosed, or represents that its use would not infringe privately owned rights. Reference herein to any specific commercial product, process, or service by its trade name, trademark, manufacturer, or otherwise, does not necessarily constitute or imply its endorsement, recommendation, or favoring by the United States Government or any agency thereof, or the Regents of the University of California. The views and opinions of authors expressed herein do not necessarily state or reflect those of the United States Government or any agency thereof or the Regents of the University of California.

The Dependence of Fracture Mechanical and Fluid Flow Properties on
Fracture Roughness and Sample Size

Y. W. Tsang and P. A. Witherspoon

Earth Sciences Division
Lawrence Berkeley Laboratory
University of California
Berkeley, California 94720

May 1982

Abstract

A parameter study has been carried out to investigate the interdependence of mechanical and fluid flow properties of fractures with fracture roughness and sample size. A rough fracture can be defined mathematically in terms of its aperture density distribution. Correlations were found between the shapes of the aperture density distribution function and the specific fractures of the stress-strain behavior and fluid flow characteristics. Well-matched fractures had peaked aperture distributions which resulted in very nonlinear stress-strain behavior. With an increasing degree of mismatching between the top and bottom of a fracture, the aperture density distribution broadened and the non-linearity of the stress-strain behavior became less accentuated. The different aperture density distributions also gave rise to qualitatively different fluid flow behavior. Findings from this investigation make it possible to estimate the stress-strain and fluid flow behavior when the roughness characteristics of the fracture are known; and conversely, to estimate the fracture roughness from an examination of the hydraulic and mechanical data. Results from this study showed that both the mechanical and hydraulic properties of the fracture are controlled by the large-scale roughness of the joint surface. This suggests that when the stress-flow behavior of a fracture is being investigated, the size of the rock sample should be larger than the typical wave length of the roughness undulations.

Introduction

In a recent paper (Tsang and Witherspoon, 1981) we developed a theoretical relationship between the nonlinear effective Young's modulus of a rough-walled fracture and its roughness profile. The theoretical model has been validated against laboratory measurements. It allows one to deduce from normal stress-displacement measurements the roughness profile of the rock fracture, and in turn to predict the fluid flow through such a fracture as a function of normal stress. In this paper we investigated many different fractures of known roughness profile to find correlations between specific features in the normal stress-displacement curve of a fracture and the actual geometric characteristics of the fracture. This systematic study lends additional insight on the interdependence of fluid flow through a fracture and the stress-displacement measurements across the fracture.

Not much information is available in the literature on the roughness characteristics of single fractures. Sharp (1970) showed an aperture frequency histogram obtained from laboratory measurements of a tension fracture. Neuzil and Tracy (1981) modeled a rough fracture using a log normal aperture frequency distribution in their theoretical work on flow through rough fractures.

Our approach assumes no specified mathematical form for the aperture distribution; it is derived from the actual joint profiles as shown in Figure 1, which is reproduced from Figure 9 of Bandis et al. (1981). It shows a selection of joint surface profiles from natural exposures of sandstone, siltstone, and limestone. If each joint surface profile were to represent both the top and bottom halves of a fracture, then different fracture apertures may be

simulated from each profile when the upper and lower joints are mismatched in varying degrees. This approach of simulating fractures from real joint profiles is suited to the purpose of our systematic study, where one needs a large sampling of fractures with known roughness characteristics, and where each fracture may be represented mathematically by an aperture distribution function. We note that in Figure 1, the roughness of each joint surface is characterized by a large-scale undulation on which is superimposed a small-scale roughness whose average amplitude and wavelength are much smaller than that of the large-scale undulation. The profiles range from rough undulation to almost smooth and planar. For our analysis, we chose fractures that are simulated from profiles 1 and 10 in Figure 1. These two profiles are distinctly different in their typical large-scale undulation amplitude; however, their small-scale roughness is similar. We computed the normal stress-displacement and stress-fluid flow characteristics of these fractures. Through our analysis, sufficient insight was gained to enable us to correlate the mechanical and hydraulic properties of the fracture to the fracture roughness. Therefore, given a rough-walled fracture, certain characteristics in the normal stress-displacement and normal stress-flow curves can be anticipated. Conversely, given normal stress-displacement and stress-flow measurements, the results of this study enable one to have an intuitive feeling as to the geometric characteristics of that rough fracture, eliminating the need for actual, lengthy mathematical calculations of our earlier approach (Tsang and Witherspoon, 1981).

Furthermore, our study indicates that it is the large-scale roughness undulation of the fracture walls, and the degree of mismatching between the

two walls of the fracture that control the shape of the normal stress-displacement curve, which in turn determines the dependence of flow on normal stress. Our investigation therefore suggests that the large-scale undulation wavelength of a fracture wall may be the key to the appropriate representative equivalent volume (REV) for stress-flow behavior of single fractures.

Method

We discussed in the introduction that each joint surface profile as displayed in Figure 1 may be considered to represent both the upper and lower joint surfaces of a fracture. Different fracture apertures may then be constructed when the upper and the lower joints are mismatched in varying degrees. Figure 2 shows four different variations that were generated from the same joint surface profile 1 in Figure 1. In Figure 2a,b,c,d, the top joint has been displaced to the right of the bottom joint by fractions varying from 0.013, 0.030, 0.056, 0.17, respectively, of the entire profile length. We have assumed that the roughness profile repeats itself, the profile lengths displayed in Figure 1 being the smallest repeating unit. The fractures in Figure 2 were constructed from the same roughness profile 1 by the above-mentioned horizontal displacement plus enough vertical separation to ensure that there was no overlap between the upper and lower profiles. If the profile for each of the fractures in Figure 2 is discretized into appropriate length units, then the fraction of discretized length units having an aperture value b will give the aperture density distribution $n(b)$, which is an appropriate mathematical description of the physical fracture. The apertures range from zero to some maximum value b_0 .

In the earlier work (Tsang and Witherspoon, 1981) we used a void description of the fracture, that is, each fracture such as shown in Figure 2 can be considered as a collection of elongated voids of length, $2d$. Assuming a spatially random distribution for the voids which make up the fracture, we derived the following relationship:

$$1 - \frac{E_{\text{eff}}}{E} \propto \langle d \rangle, \quad (1)$$

where E_{eff} is the effective Young's modulus of the rock with the fracture, E is the Young's modulus of the intact rock, and $\langle d \rangle$ is one-half the crack length averaged over all the voids. The physical picture implied by (1) is illustrated in Figure 3, which portrays a portion of fracture at increasing levels of applied stress. Under increasing load, the deformation of the voids causes more areas between the top and bottom of the fracture to come in contact and leads to a decrease in $\langle d \rangle$. This process results in a gradual increase of the effective modulus with increasing load according to (1). Equation (1) therefore provides a bridge between the mechanical properties of a fractured rock and the geometrical characteristics of the fracture. We shall show in the following that, given a fracture for which the aperture density distribution has been defined, we can calculate the fracture mechanical properties.

When measurements are made on intact rock over a thickness l , then by definition,

$$E = l \frac{d\sigma}{d(\Delta V_r)} \quad (2)$$

and for a rock with a single fracture, one has

$$E_{\text{eff}} = l \frac{d\sigma}{d(\Delta V + \Delta V_r)} \quad (3)$$

where ΔV_r is the deformation of the intact rock and ΔV , the closure of the fracture. Note that whereas ΔV_r will be proportional to l , ΔV is a property intrinsic to the fracture and is independent of l . Therefore, an evaluation of E_{eff} in (3) from stress-displacement measurements depends on l and is nonunique. That is, the larger the l chosen, the more difficult it will be to distinguish the effect of the presence of the fracture from the overall mechanical property of the rock.

If the modulus E of the intact rock is a constant, equations (2) and (3) reduce to

$$\int d\sigma = \frac{E}{l} \int \frac{E_{\text{eff}}/E \, d(\Delta V)}{(1 - E_{\text{eff}}/E)}. \quad (4)$$

The integrand on the right-hand side of (4) can be computed from the geometry of the fracture profile, which is represented by the aperture density $n(b)$ as determined at zero stress; that is, when the fracture closure ΔV is zero. As the fracture closes, ΔV increases and each aperture is reduced the amount ΔV . All apertures in $n(b)$ having values of b less than ΔV now become zero. Therefore the fractional contact area, ω , at each fracture closure is

$$\omega = \int_0^{\Delta V} n(b) \, db. \quad (5)$$

For a spatially random distribution of voids, the average half-crack length $\langle d \rangle$ is inversely proportional to the fractional contact area. Since $\langle d \rangle$ is related to E_{eff}/E from (1), the integral in (4) may be evaluated numerically for any given $n(b)$. We should point out that the proportionality sign in (1) implies that a reference crack length at zero stress is needed. Since the entire length of profile 1 shown in Figure 1 contains approximately three large-scale undulation wavelengths, we have chosen the reference crack length to be one-third of the entire profile in our computations.

Correlation Between Fracture Roughness and Stress Displacement Characteristics

The aperture density $n(b)$ versus aperture b in the absence of applied normal stress for the four different fractures shown in Figures 2a,b,c,d are plotted respectively in Figures 4 through 7. The same horizontal and vertical scales are used for all the figures so that a meaningful comparison may be made among them. Recall that all the fractures in Figure 2 originate from the same joint roughness profile 1, they differ only in the amount of lateral mismatching between the top and bottom. Figures 4 through 7 show that the larger the lateral displacement in forming the fracture, the larger is the value of the maximum aperture b_0 in the fracture. Though the aperture distributions show a lot of noise arising from the small-scale roughness of the joint surface, an overall envelope for each distribution is discernible. The envelopes arise from the large-scale undulation of the joint, their shapes range from a narrow peaked distribution on Figure 4 corresponding to the fracture in Figure 2a to a flat, almost uniform distribution on Figure 7 for the fracture shown in Figure 2d.

The characteristics of the stress versus fracture closure curves may be correlated to the aperture distribution. In Figures 4 through 7, the normal stress σ versus fracture closure ΔV for the four different fractures shown in Figures 2a,b,c,d are also plotted together with the distributions of $n(b)$ versus b . The stress is left in relative units for the purpose of this study. According to equation (4), actual values of σ may be obtained when the Young's modulus (E) of the intact rock and the actual conditions of measurements (l) are known. The flat tail of the σ versus ΔV curve at small ΔV (Fig. 4) corresponds to low-aperture densities $n(b)$ at small apertures b . Therefore, for small ΔV , the fracture contact area increases very slowly (see (5)) as ΔV is increased. Also, the average crack length remains large (see Fig. 3), hence E_{eff} remains small according to (1) and the nearly flat slope of $d\sigma/d\Delta V$ results. As $n(b)$ peaks, the contact area increases rapidly, causing the average crack length to decrease rapidly, giving rise to a steady increase of the slope $d\sigma/d\Delta V$. As $n(b)$ decreases again beyond the peak, the slope $d\sigma/d\Delta V$ approaches a constant. These correlations between the shape of the σ versus ΔV curve and the shape of $n(b)$ are consistently seen in Figures 4 through 7. When the aperture density is appreciable at small b (Fig. 6), the flat tail of the σ versus ΔV curve, so prominent in Figure 4, has all but disappeared.

We note in the progression from Figure 4 through Figure 7 that as the mismatch between the top and lower joints increases (Figs. 2a through 2d), respectively, the aperture distribution broadens and the variation of σ with ΔV becomes less steep. This difference in behavior between a well-mated joint and an ill-mated joint had been seen for a granodiorite specimen (Goodman,

1976). The maximum allowed fracture closure ΔV should equal b_0 , the maximum aperture of the fracture at zero applied load. At this value of ΔV , the fracture is totally closed and σ versus ΔV is of course vertical. However, in the cases where the aperture distribution peaks sharply, σ versus ΔV can become near-vertical long before the value of maximum closure is reached. This is because the aperture distribution peak can occur at a value b anywhere between zero and the maximum b_0 . Then, corresponding to the post-peak aperture distribution decline, even at values of b considerably below b_0 the fractional fracture contact area can be very nearly one and the average crack length nearly zero, implying that the effective modulus of the fractured rock will be almost identical to that of the intact rock. This is the case in Figures 4 and 5 where the aperture distributions are peaked. In these figures the $n(b)$ versus b curve extends to the maximum aperture b_0 , whereas the σ versus ΔV curve terminates at a value ΔV considerably below that of its maximum allowed value b_0 , beyond this value of ΔV at which the calculated curve terminates, the slope of σ versus ΔV approaches infinity. For broad and flat aperture distributions such as those in Figures 6 and 7, the slope of σ versus ΔV remains finite until ΔV almost reaches b_0 .

The well-matched fracture characterized by a peaked aperture distribution with small b_0 (e.g., Fig. 4) also differs from an ill-matched fracture characterized by a flat aperture distribution with larger b_0 (e.g., Fig. 7) in the fractional contact area variation with fracture closure. Curve (a) in Figure 8 shows the fractional fracture contact area variation for the most well-matched fracture (Fig. 2a). The s-shaped curve demonstrates that the

fractional fracture contact area remains small and the fracture is soft at small ΔV , then the contact area increases rapidly becoming almost 1 long before the maximum possible closure b_0 is reached. This s-shaped variation corresponds to the initial zero slope on Figure 4 and the subsequent rapid rise in slope of the σ versus ΔV curve. The almost linear curve (d) in Figure 8 corresponds to the most ill-matched fracture (Fig. 2d) characterized by the broad aperture distribution of Figure 7. Since fractional contact area at a fracture closure is mathematically the integral of aperture density from aperture 0 to aperture ΔV , one expects that a totally flat aperture distribution (completely random aperture distribution) should give a 45° straight line for the fractional contact area variation with fracture closure. Curve (d) in Figure 8 for the most ill-matched fracture gives almost this shape. This linear variation corresponds to the slow and steady rise in slope of the σ versus ΔV curve in Figure 7.

Stress and aperture distribution calculations were also carried out using the joint surface profile 10 in Figure 1. Fractures were formed using lateral displacements of the same magnitudes as in the calculations for profile 1. Whereas profiles 1 and 10 have comparable small-scale roughness and average large-scale undulation wavelength, they differ most distinctly in their typical large-scale undulation amplitude. By virtue of the smaller undulation amplitude in profile 10, one may say that the joint in profile 10 is smoother than that in profile 1. Each fracture constructed from profile 10 has apertures much smaller than the corresponding fracture constructed from profile 1. This result is consistent with our intuition that a smoother walled fracture

should give rise to smaller overall range of fracture apertures. Figure 9 shows the $n(b)$ versus b and σ versus ΔV curves for a fracture constructed from profile 10 by the least lateral displacement. This figure should be compared with Figure 4 where curves are shown for a fracture constructed from profile 1 by the same amount of lateral displacement. (Here we must point out that profiles 1 and 10 in fact belong to different rock types and therefore possess different Young's moduli. However, for the purpose of this study, we are specifically interested in the effect of fracture roughness on mechanical properties; so we borrow profiles 1 and 10 from the work of Bandis et al. (1980) and assume that they are joints of the same rock type differing only in their geometrical characteristics. This justifies the comparison between Figure 4 and Figure 9.) The distinction between Figure 4 and Figure 9 may be most simply stated in mathematical terms. In Figure 4, the square root of the variance of $n(b)$ is smaller than the mean of the distribution; whereas in Figure 9, the square root of the variance is larger than the mean of the distribution. The values of $n(b)$ for b less than zero are eliminated since negative apertures are nonphysical, thus giving rise to the skewed appearance of the aperture distribution in Figure 9. Physically, the difference in appearance between Figures 4 and 9 are accounted for as follows. The distribution of Figure 9 results because the fractures formed from profile 10 are more planar due to the smaller undulation amplitudes. Since there is appreciable density $n(b)$ at the zero end of the aperture distribution, contact area increases immediately as the fracture closure is increased from zero, therefore the feature of a flat tail in the σ versus ΔV curve at small ΔV found in the rougher fractures formed from profile 1 (e.g., Fig. 4) is absent here in

the more planar fractures from profile 10 (e.g., Fig. 9). The absence of a long flat tail at small ΔV in the σ versus ΔV curve and the overall smaller fracture apertures with a skewed aperture distribution are the prominent features that differentiate a more planar fracture from an undulation fracture. In other respects, the σ versus ΔV curves correlate to the aperture density in a similar fashion as in the case of profile 1: the broadening of the aperture density and the less steep rise of σ versus ΔV as the mismatch between the upper and lower joints increases.

The above calculations lead to an understanding of the general relationship between fracture roughness and the fracture mechanical property under normal stress. Mathematically, a well-matched fracture (such as Fig. 2a) gives rise to an aperture distribution that has a narrow and peaked envelope (Fig. 4), whereas an ill-matched fracture such as Figure 2d gives rise to an aperture distribution that has a broad and flat envelope (Fig. 7). The large-scale roughness determines the shape of the aperture distribution envelope. The small-scale roughness of the fracture wall contributes to the background noise of the aperture distributions in Figures 4 through 7. Since the features in the σ vs ΔV curves can be generally correlated to the shape of the aperture distribution envelope, it is the large-scale roughness of the fracture walls that controls the mechanical behavior of the fracture.

Fracture Fluid Flow Variation with Normal Stress

We have shown (Tsang and Witherspoon, 1981) that the fluid flow per unit head through a fracture at each stage of fracture closure ΔV varied as $\langle b^3(\Delta V) \rangle$, where

$$\langle b^3(\Delta V) \rangle = \int_{\Delta V}^{b_0} n(b)(b - \Delta V)^3 db \quad (6)$$

and $n(b)$ denotes the fracture aperture distribution in the absence of applied normal stress. Since the variation of σ versus ΔV is given in equation (4), the dependence of fluid flow on applied normal stress may be calculated. The results for the four fractures (Figs. 2a-2d) are shown in Figure 10. Recall that fractures 2a through 2d are all derived from the same joint profile 1 in Figure 1, but with increasing amount of mismatching between the top and bottom walls of the fracture. The flows at zero applied normal stress bear the ratio 1 : 2.9 : 4.8 : 35 as the mismatch increases from fractures 2a to 2d. This indicates that in the absence of asperity breakage, the geometrical characteristics of the fracture alone dictate that the flow through an initially matched fracture will increase under shear strain. Fracture 2d represents a mismatch of about half an undulation wavelength between the top and bottom joints. Further shear displacement will cause the overall fracture apertures to decrease and we expect the flow also to decrease.

In Figure 10 the flows, Q , per unit pressure head are all normalized to one at zero stress level. The stresses can again be left in arbitrary units for the purpose of this study. The extremely sharp drop of flow at small

stresses for fracture 2a reflects the mechanical softness of a well-matched fracture at the initial stages of loading, the decrease of flow with stress becomes progressively less rapid as the fractures become less well-matched. The wiggles in the curves in Figure 10 arise from the small-scale roughness of the fracture wall. The overall shapes of the curves are governed by the large-scale undulation of the fractures. The variation of Q per unit head with σ in Figure 10 may be separated into three regions: (1) an initial rapid linear drop at small stress, (2) slow but nonlinear variation with increasing stress, and (3) the asymptotic behavior at large stresses. The initial sharp drop of flow per unit head in region (1) corresponds to the flat tail in the σ versus ΔV curve such as shown in Figure 4 and is characteristic of a well-matched fracture.

Calculations also show that the flow per unit head through the fracture approaches some limiting value greater than zero at large stresses; and the more mismatched the undulating fracture, the smaller is this limiting value of flow. To illustrate this, Figure 10 is replotted in Figure 11 with the flow per unit head put into logarithmic scale. The convenient scale of length unit cubed is used for the flow by virtue of equation (6). At zero applied stress, the fluid flow through the most mismatched fracture 2d is largest since it has the largest overall apertures; however, at large stresses, the flow for the same mismatched fracture takes on the smallest value. The point of termination for each curve in Figure 11 is governed by the value of stress beyond which the σ versus ΔV curve (Fig. 4 through Fig. 7) becomes near-vertical, as discussed earlier, implying that very little fracture closure will occur

beyond this value of stress where each curve in Figure 11 terminates, and that the values of flow where the curves terminate are indicative of the nonzero limiting values. Figures 4 through 7 indicate that the more mismatched the fracture, the closer is the point of termination for σ versus ΔV curves to the maximum possible closure b_0 ; hence the smaller is the limiting value of flow for the more mismatched fracture.

The nonzero limiting values of flow per unit head at high stress are consistent with experimental evidence [Kranz et al., 1979] that fractures remain open for fluid flow even up to effective stresses of 200-300 MPa. This is also not surprising if we consider the physics that is involved. Recall from equations (1) and (2) that over a thickness l , E is defined in terms of the rock displacement ΔV_r with stress and E_{eff} is defined in terms of the total displacement ΔV_t , which is the sum of the rock displacement and the fracture closure. One may separate this thickness l further into two components, one is the immediate area around the fracture, on the order of thickness b_0 , which we shall call l_1 . The modulus of this fracture region will be denoted by E_1 . The other component is the rock away from the immediate vicinity of the fracture, with thickness $(l - l_1)$ and intact rock modulus E . When normal stress is applied to l , the respective displacements in the two regions are ΔV and ΔV_r . If a two-springs analog is used to describe the system, it is straight-forward to show that

$$\frac{l}{E_{\text{eff}}} = \frac{l_1}{E_1} + \frac{(l - l_1)}{E} \quad (7)$$

In the void description of the fracture, when the crack lengths are long,

$E_{\text{eff}}/E \ll 1$, implying that the fracture region (E_1) will be so soft that the measured total displacement ΔV_t would be dominated by the fracture closure ΔV . However, as the stress level increases, the crack lengths shorten and E_{eff}/E approaches 1, then E_1 is no longer significantly different from the intact rock modulus E . In which case, to separate l into two regions and to describe it by the two-springs analog is artificial. In fact, the response of the region l to external load is simply that of one 'spring', that corresponding to the rock. Within the fracture, the response to external load is from the 'shortening' of those asperities already in contact, rather than further closure to bring more asperities into contact. Whereas in the initial stage of applied load the 'void' description of the fracture predict rapid closure of the fracture, now at larger stresses the shortening of the asperities already in contact with increasing load implies that the fracture remains open for fluid flow even at very high stresses.

That the curves in Figure 11 should take on such different shapes for the four different fractures is of interest. Since the curves 11(a) through 11(d) correspond to fractures with their aperture distributions ranging from sharply peaked to very broad and flat, then the different shapes of these logarithms of flow per unit head versus stress curves may very well be a potential tool for guessing the aperture characteristics of the fracture in question. Iwai's (1976) flow data for very well-matched rough fractures indeed take on the shape of curve (a) in Figure 11, but much more experimental evidence is needed to substantiate our hypothesis here.

The Critical Role of Sample Size to Stress and Flow Measurement

In this systematic study, we have arrived at the conclusion that the mechanical and hydraulic properties of a fracture under normal stress can be correlated to the geometrical characteristics of the fracture. The large-scale roughness of a well-matched fracture is characterized mathematically by a narrow and peaked aperture distribution; that of an ill-matched fracture is characterized by an aperture distribution that is broad and flat. The small-scale roughness of the fracture wall contributes to the background noise of the overall shape of the aperture distribution. Since the features in σ versus ΔV and Q versus σ curves have been shown to correlate to the shape of the aperture distribution, it is the large-scale roughness of the fracture walls that control the mechanical and hydraulic behavior of the fracture. It is clear then that rock samples smaller than a typical large-scale undulation wavelength do not represent the fracture roughness properly, and spurious results due purely to 'size' can occur when such small samples are used in stress and flow measurements. In other words, the large-scale undulation wavelengths of the fracture wall may be a good measure of the "representative equivalent length" for the scale effect in stress and flow measurements. Figure 1 shows that the undulation wavelengths range from about 12 cm for profiles numbered 1, 5, 10 to perhaps 70 cm in profile 6. The other profiles have wavelengths on the order of 30 cm. If Figure 1 is a good sampling of typical rock profiles, then our study seems to suggest that in order to obtain a data base from which laboratory experimental results may be extrapolated to field situations, rock samples much larger than those conventionally employed in laboratory stress-strain and stress-flow measurements are called for.

Conclusions

Conclusions drawn from this investigation in many ways coincide with what one will intuitively expect with regard to the relationship between fracture roughness characteristics and its mechanical and hydraulic properties. This systematic study therefore supplies the theoretical basis for our physical intuition. We summarize in the following our findings from this study, they are:

- (1) The roughness of a fracture wall may be characterized by a small-scale roughness superposed on a large-scale undulation. It is the large-scale undulation in the fracture wall roughness that determines the shape of the aperture density distribution and therefore controls the mechanical and hydraulic properties.
- (2) When the fractures are well matched, the aperture distribution is narrow and peaked; with increasing mismatching, the aperture distribution broadens and flattens. In mathematical terms, both the variance and the mean of the aperture distribution increase as the fracture becomes more mismatched. The aperture distribution for a perfectly matched rough fracture is a delta function, which is also the mathematical description for the conventional parallel flat plate description of fractures. For mismatched fractures, as the ratio of the undulation amplitude and wavelength of the fracture wall decreases, that is, in going from rough-walled to planar fractures, the overall aperture decreases and the square root of the variance becomes larger than the mean of the distribution.

- (3) The peaked aperture distribution of a well-matched fracture gives rise to very soft mechanical properties at low stresses and therefore very non-linear stress-fracture closure behavior. As the fracture becomes more mismatched, the nonlinearity of the stress-fracture closure behavior becomes less accentuated.
- (4) The fracture hydraulic property follows closely the fracture mechanical property. The calculations for fractures 2a - 2d indicate that dilatancy occurs when a fracture undergoes shear displacement (under zero loading conditions). The flow should first increase, reaching a maximum when the mismatch between the upper and lower joints is about 1/2 of the large-scale undulation wavelength, and then decrease with further shear displacement. When only normal stress is present, the soft mechanical behavior gives rise to a sharp drop of flow with stress, hence the more well-matched the fracture the sharper the drop of flow with stress at low levels of applied normal load. The different shapes of the curves of logarithms of flow per unit head versus stress may serve as a "fingerprinting tool" for the fracture roughness characteristics.

Equipped with the findings from this investigation one can now make qualitative predictions about the expected stress-fracture closure behavior and expected stress-flow behavior of any fracture from an examination of the fracture wall roughness and the degree of fracture mismatching alone. On the other hand, hydraulic and mechanical data can also give one the clue to the roughness characteristics of a fracture.

That the large-scale undulation wavelength of the fracture wall seems to be the key to the representative equivalent length for fracture mechanical and hydraulic properties is significant. This implies that if a representative undulation wavelength can be determined for the fractures in the field, then perhaps laboratory experiments on the suitably sized samples of about 1.5 to 2 undulation wavelengths may be sufficient to provide flow and stress data that can be transferrable to the field situation.

Acknowledgements

This work was supported by the U. S. Department of Energy under Contract Number DE-AC03-76SF00098.

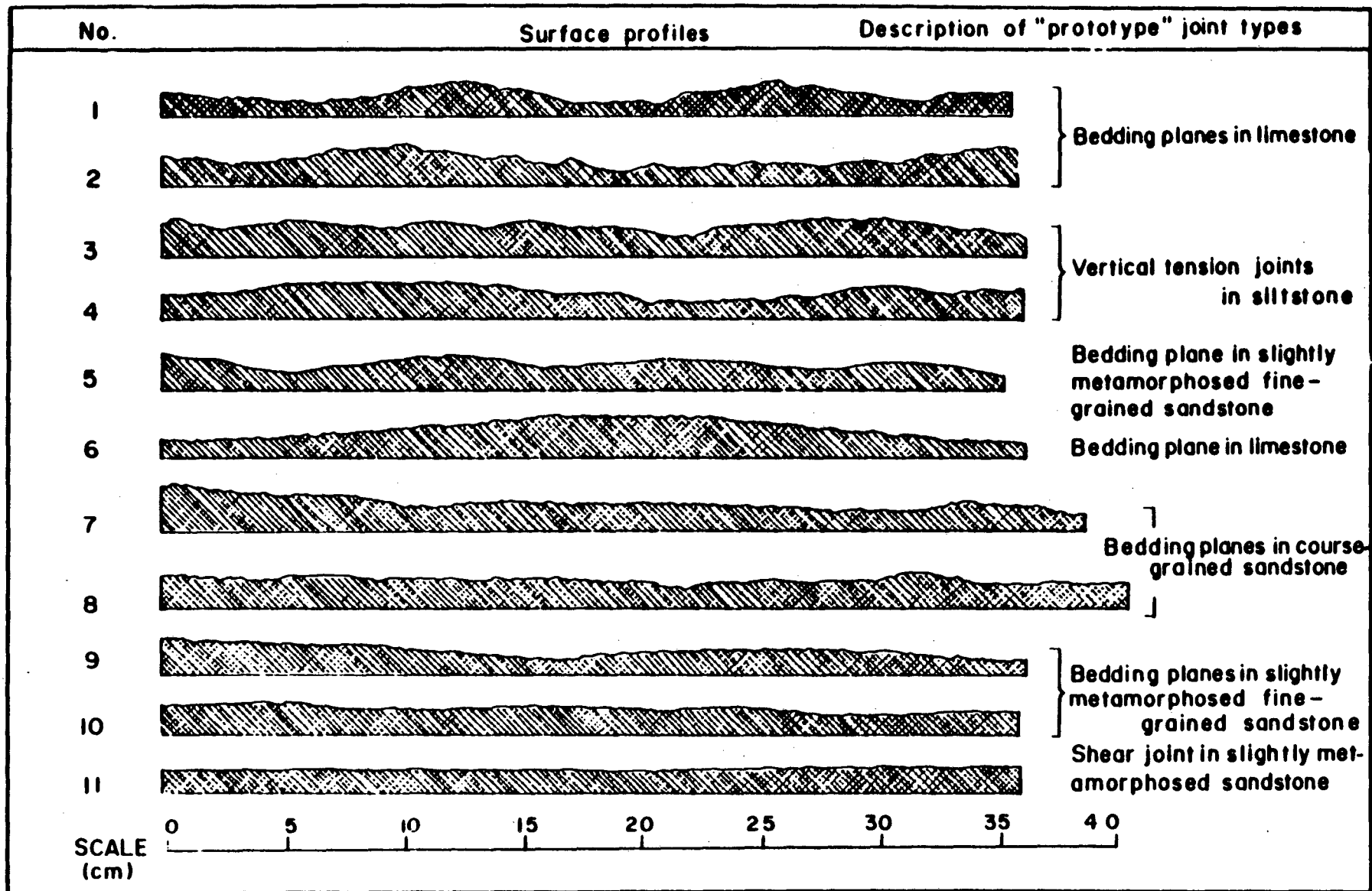
References

- Bandis, S., Lumisden, A. C., and Barton, N. R., Experimental Studies of Scale Effects on the Shear Behavior of Rock Joints. Int. J. Rock Mech. Min. Sci., 18, 1-21, 1981.
- Iwai, K., Fundamental Studies of the Fluid Flow Through a Single Fracture. Ph.D. thesis, University of California, Berkeley, 1976.
- Kranz, R. L., Frankel, A. D., Engelder, T., and Scholz, C. H., The Permeability of Whole and Jointed Barre Granite. Int. J. Rock. Mech. Min. Sci., 16, 225-234, 1979.
- Neuzil, C. E., and Tracy, J. V., Flow Through Fractures. Water Resourc. Res. 17, 191-199, 1981.
- Sharp, J. C., Fluid Flow Through Fissured Media, Ph.D. thesis, Imp. Coll. of Sci. and Technol., London, 1970.
- Tsang, Y. W., and Witherspoon, P. A., Hydromechanical Behavior of a Deformable Rock Fracture Subject to Normal Stress, J. Geophys. Res., 86(B10), 9287-9298, 1981.

List of Figures

- Figure 1. Selection of typical joint surface profiles (after Bandis, Lumsden, and Barton, 1981).
- Figure 2. Four figures generated from the surface profile number 1 of Figure 1.
- Figure 3. Deformation of 'voids' in a sequence of increasing normal stress.
- Figure 4. Fracture aperture distribution and stress-fracture closure variation for fracture 2a.
- Figure 5. Fracture aperture distribution and stress-fracture closure variation for fracture 2b.
- Figure 6. Fracture aperture distribution and stress-fracture closure variation for fracture 2c.
- Figure 7. Fracture aperture distribution and stress-fracture closure variation for fracture 2d.
- Figure 8. Fractional contact area as a function of fracture closure for fractures 2a and 2d.
- Figure 9. Fracture aperture distribution and stress-fracture closure variation for fracture generated from surface profile 10 of Figure 1.
- Figure 10. Normalized fluid flow per unit pressure head variation with applied normal stress for fractures 2a-2d.
- Figure 11. Logarithm of fluid flow per unit pressure head versus applied normal stress for fractures 2a-2d.

LARGE SCALE UNDULATION + SMALL SCALE ROUGHNESS



XBL 828-2353

Figure 1. Selection of typical joint surface profiles (after Bandis, Lumsden, and Barton, 1981).

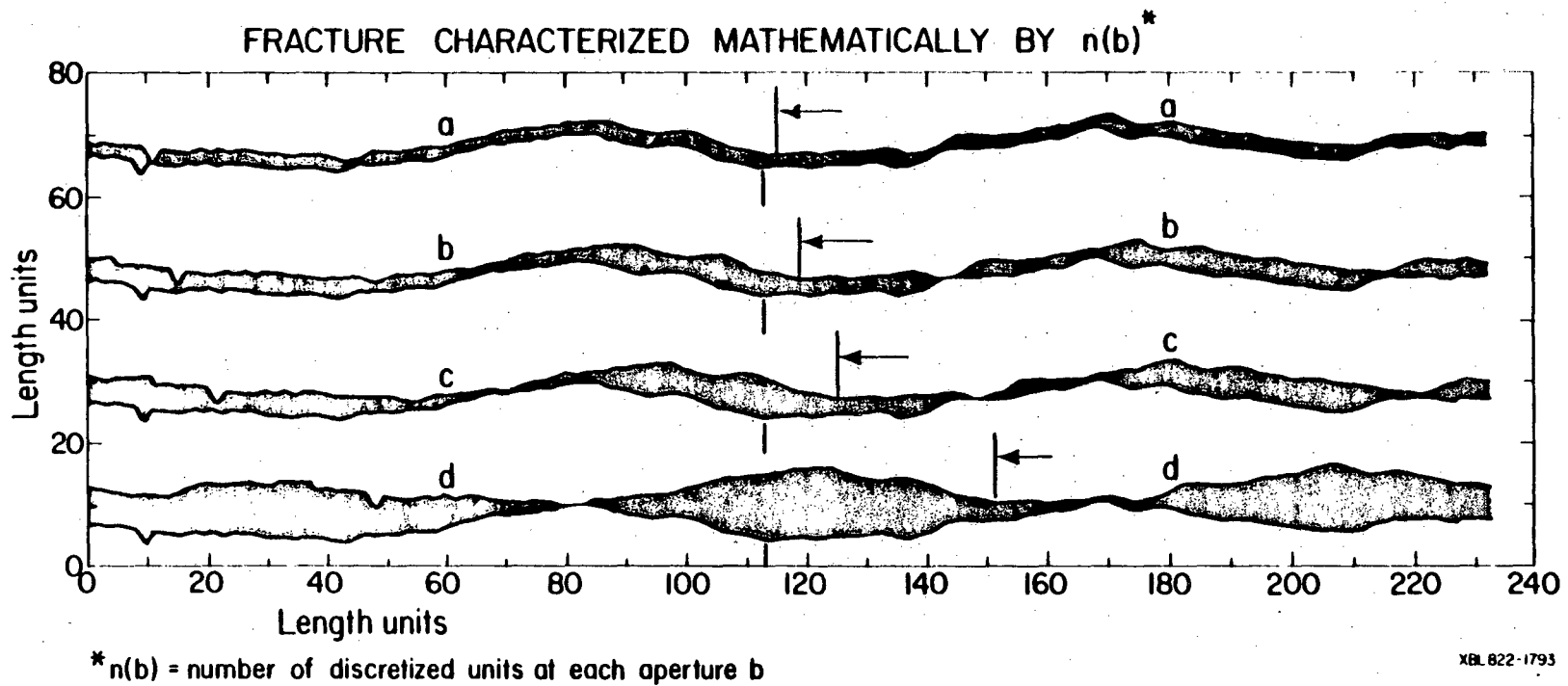
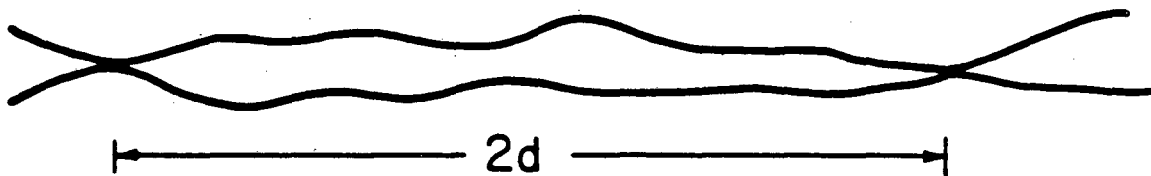
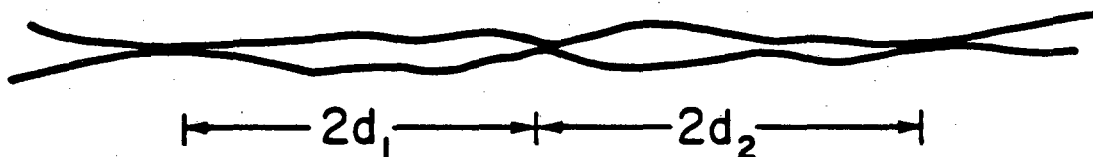


Figure 2. Four figures generated from the surface profile number 1 of Figure 1.

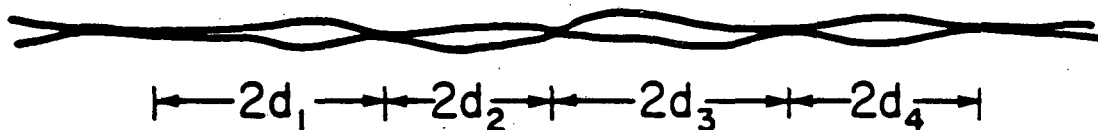
(a) at normal stress σ_1



(b) at normal stress $\sigma_2 > \sigma_1$

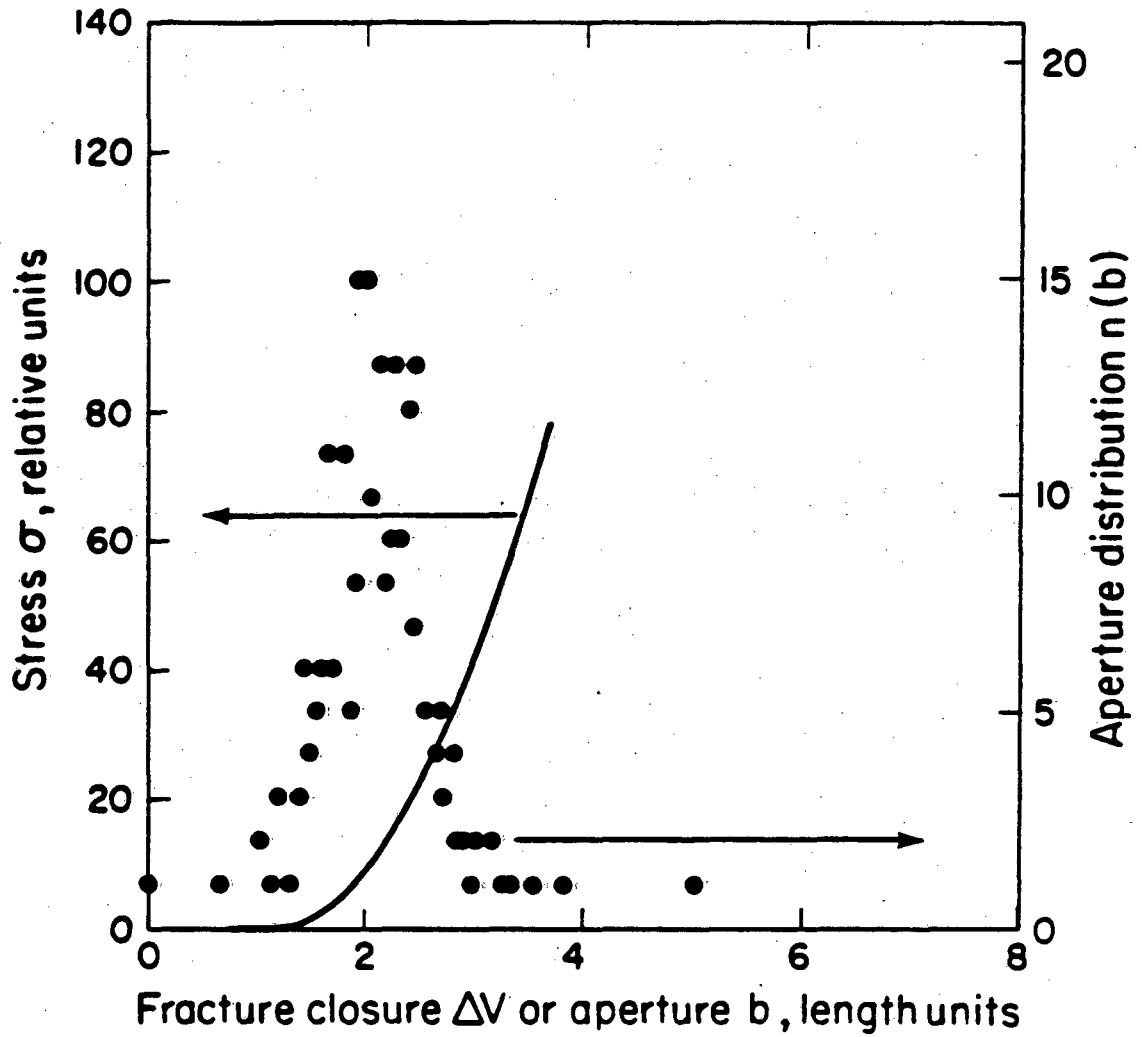


(c) at normal stress $\sigma_3 > \sigma_2$



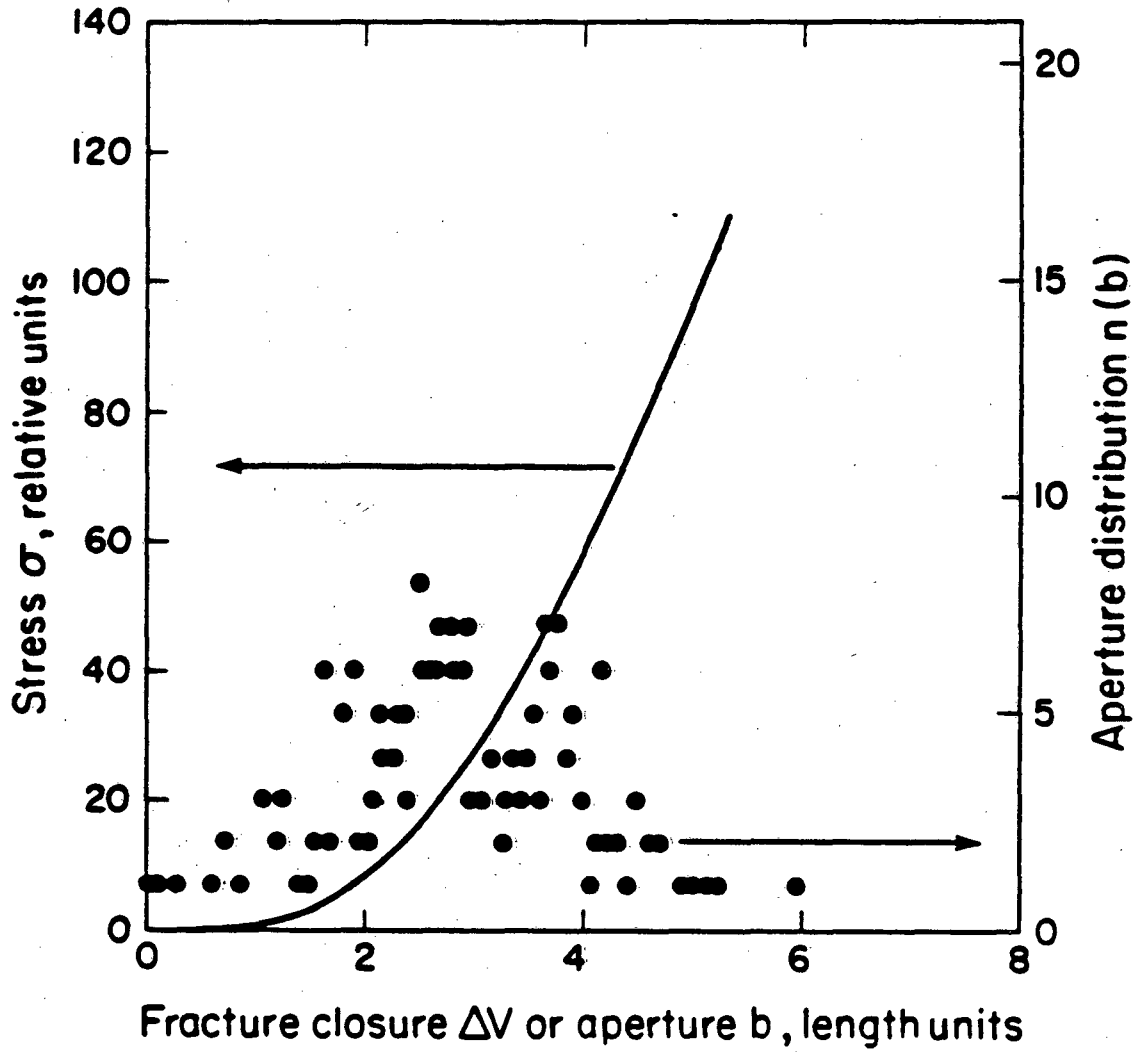
XBL 8011-2975

Figure 3. Deformation of 'voids' in a sequence of increasing normal stress.



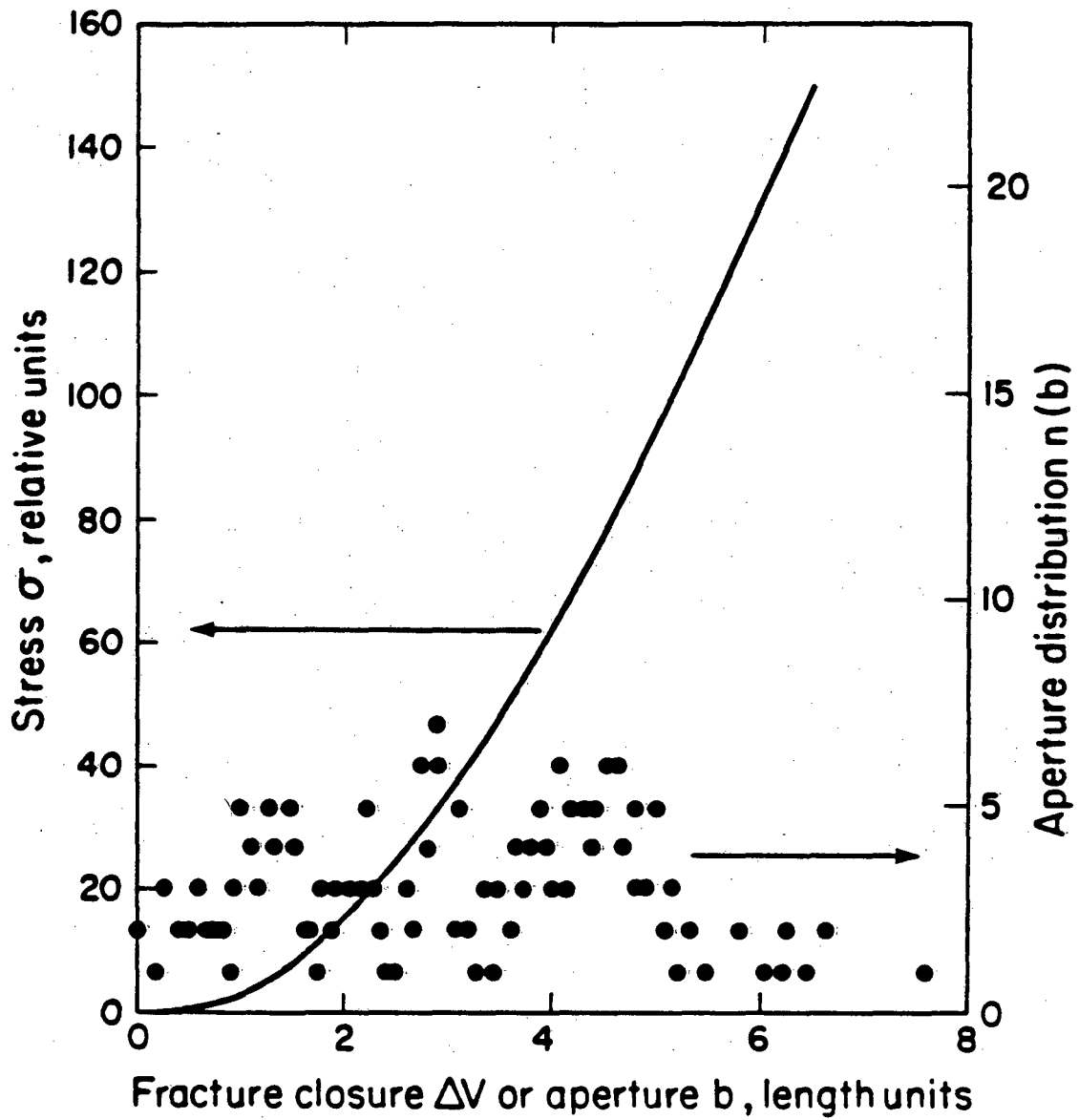
XBL822-1795

Figure 4. Fracture aperture distribution and stress-fracture closure variation for fracture 2a.



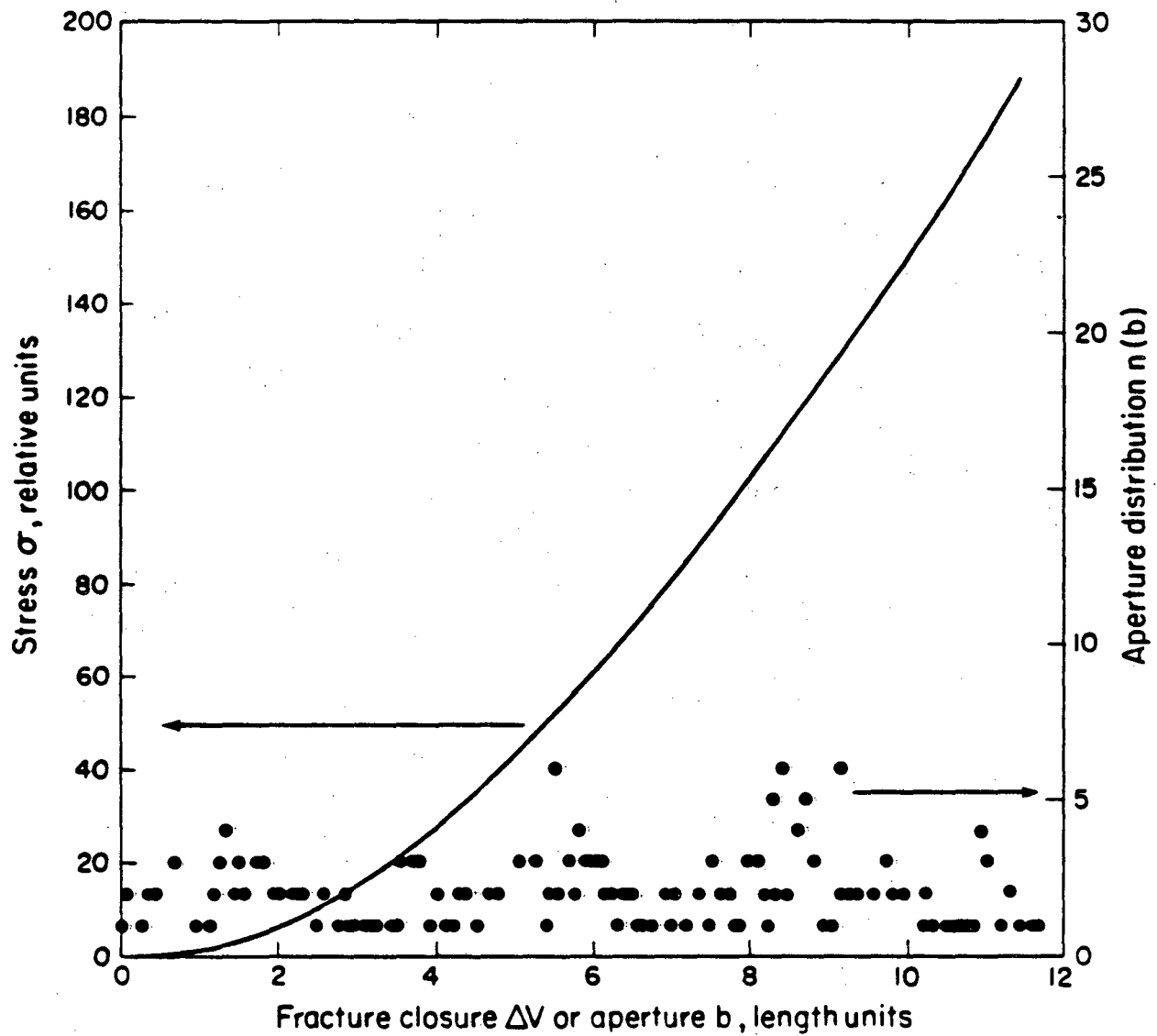
XBL822-1796

Figure 5. Fracture aperture distribution and stress-fracture closure variation for fracture 2b.



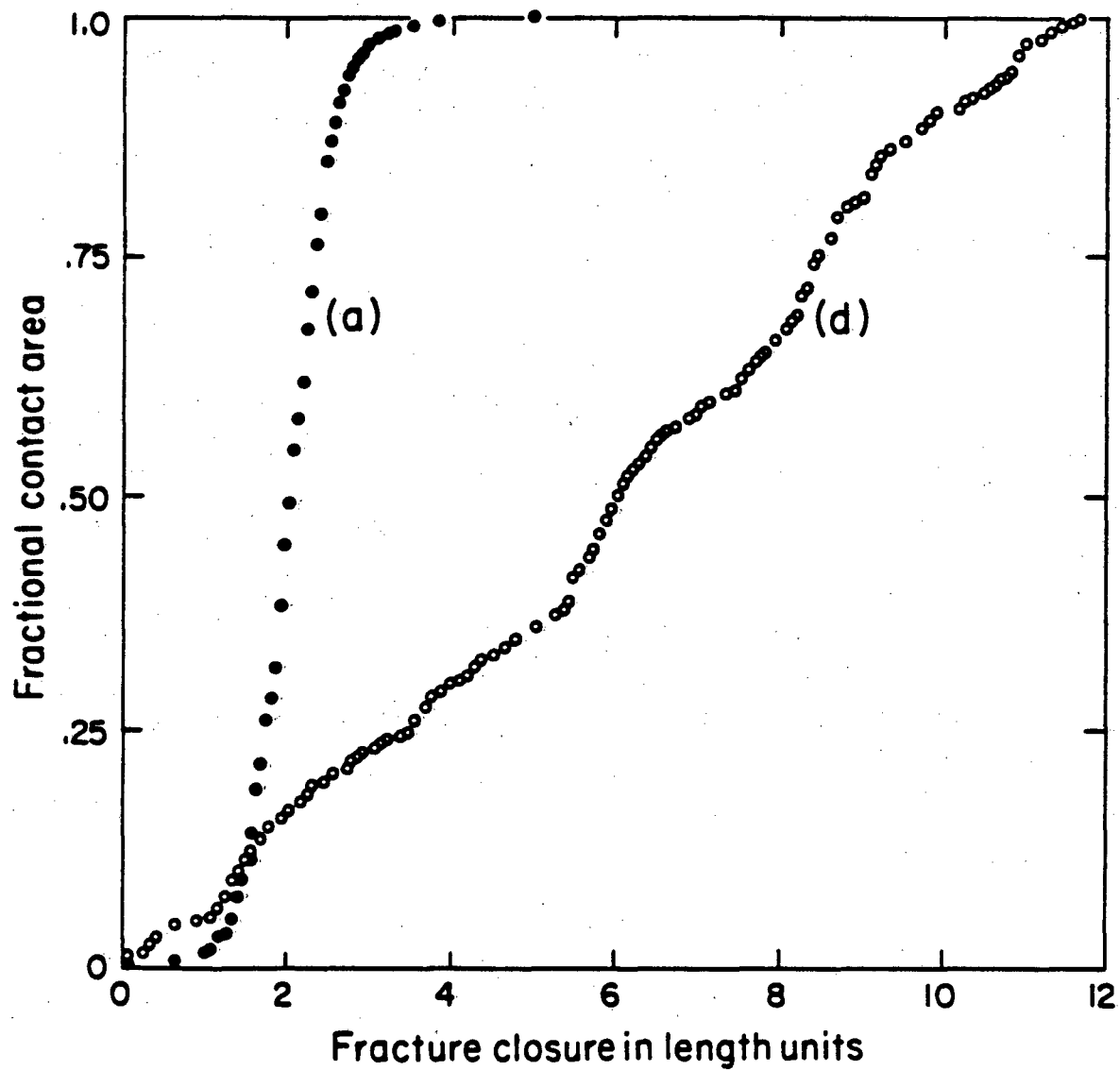
XBL 822-1797

Figure 6. Fracture aperture distribution and stress-fracture closure variation for fracture 2c.



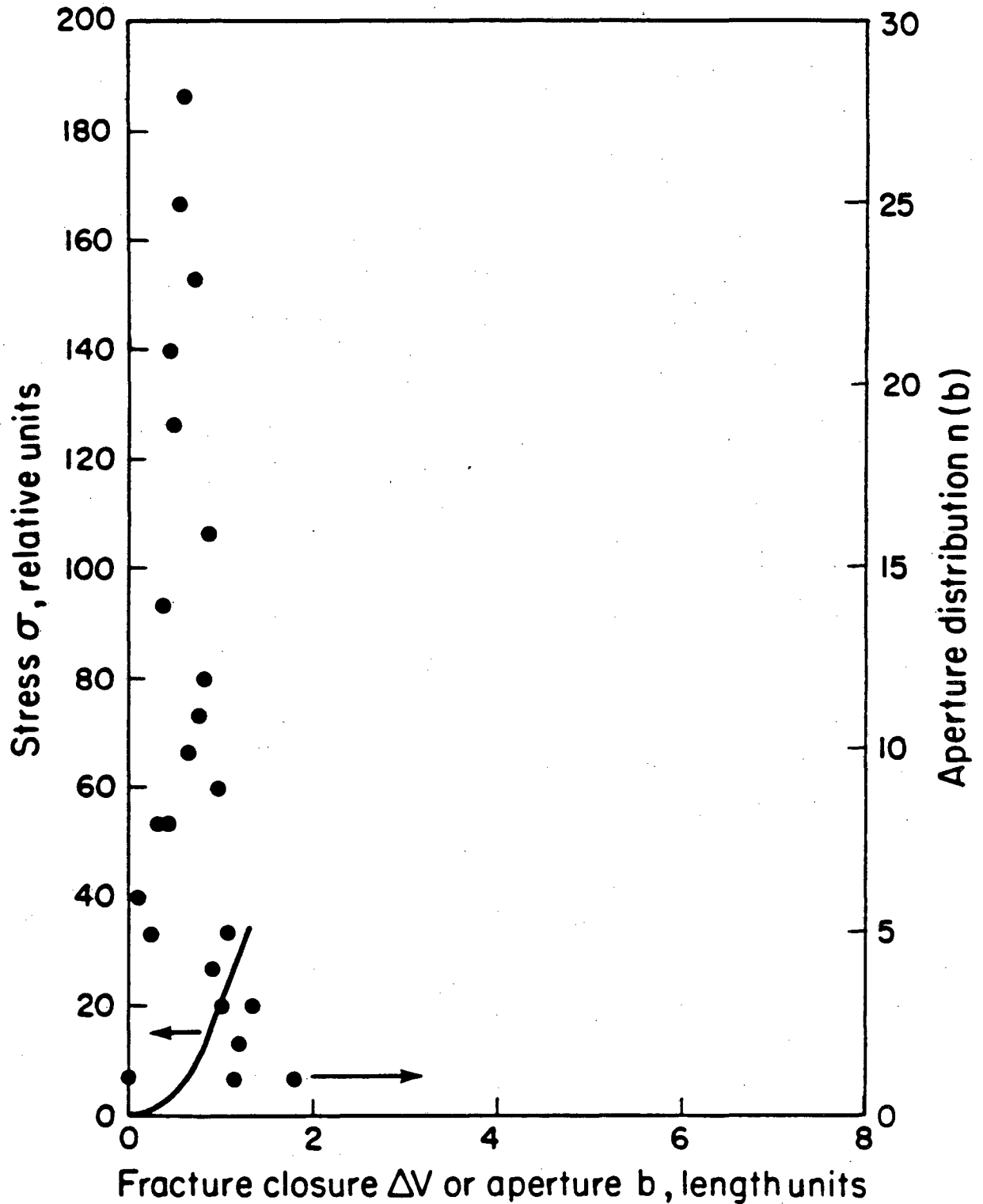
XBL 822-1798

Figure 7. Fracture aperture distribution and stress-fracture closure variation for fracture 2d.



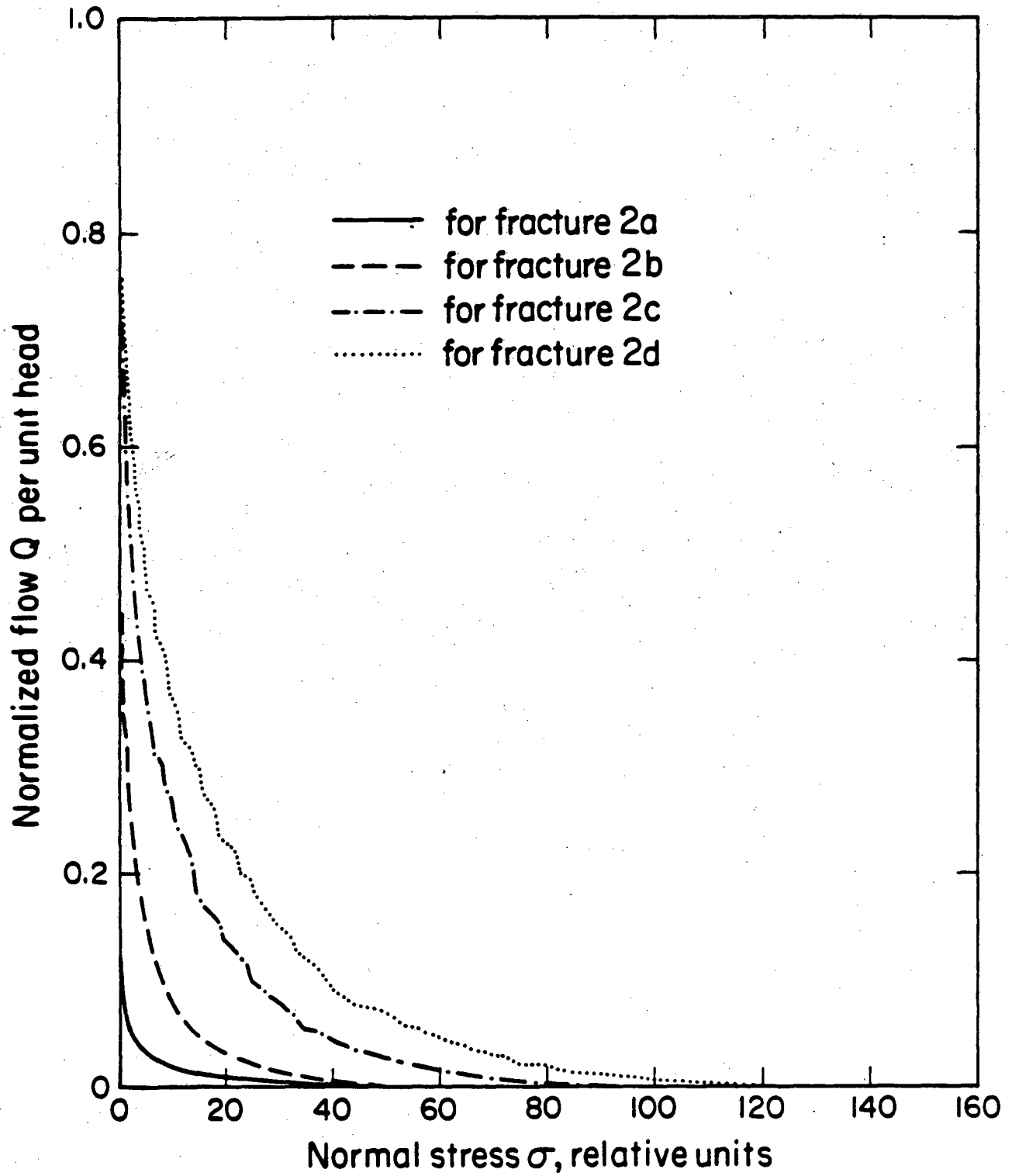
XBL 822-1870

Figure 8. Fractional contact area as a function of fracture closure for fractures 2a and 2d.



XBL 824-2118

Figure 9. Fracture aperture distribution and stress-fracture closure variation for fracture generated from surface profile 10 of Figure 1.



XBL 824-2120

Figure 10. Normalized fluid flow per unit pressure head variation with applied normal stress for fractures 2a-2d.

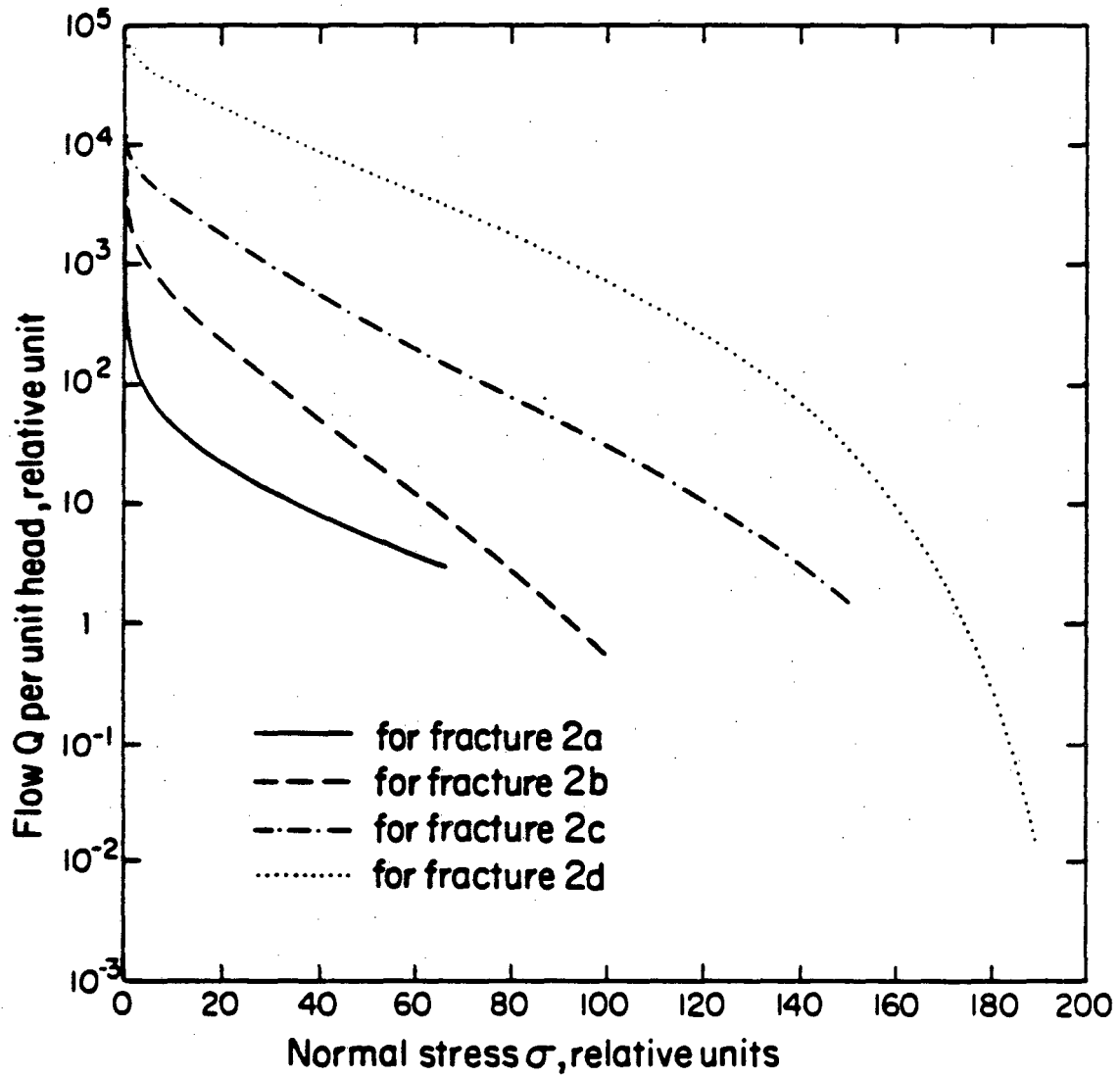


Figure 11. Logarithm of fluid flow per unit pressure head versus applied normal stress for fractures 2a-2d.

This report was done with support from the Department of Energy. Any conclusions or opinions expressed in this report represent solely those of the author(s) and not necessarily those of The Regents of the University of California, the Lawrence Berkeley Laboratory or the Department of Energy.

Reference to a company or product name does not imply approval or recommendation of the product by the University of California or the U.S. Department of Energy to the exclusion of others that may be suitable.

TECHNICAL INFORMATION DEPARTMENT
LAWRENCE BERKELEY LABORATORY
UNIVERSITY OF CALIFORNIA
BERKELEY, CALIFORNIA 94720